Solar Radiation Transfer Through a Subarctic Shrub Canopy

Authors: Bewley, D., Pomeroy, J. W., and Essery, R. L. H.

Source: Arctic, Antarctic, and Alpine Research, 39(3) : 365-374

Published By: Institute of Arctic and Alpine Research (INSTAAR), University of Colorado

URL: https://doi.org/10.1657/1523-0430(06-023)[BEWLEY]2.0.CO;2

Arctic, Antarctic and Alpine Research, Vol. 39, No. 3, 2007, pp. 365–374

Solar Radiation Transfer through a Subarctic Shrub Canopy

*D. Bewley**†
*J. W. Pomeroy**‡ *and*
*R. L. H. Essery**

*Centre for Glaciology, Institute of Geography and Earth Sciences, University of Wales, Aberystwyth SY23 3DB, U.K.
†Present address: Department of Forest Resources Management, Faculty of Forestry, University of British Columbia, Vancouver, V6T 1Z4, Canada
‡Corresponding author. Present address: Centre for Hydrology, Department of Geography, University of Saskatchewan, 117 Science Place, Saskatoon S7N 5C8, Saskatchewan, Canada
john.pomeroy@usask.ca

Abstract

Much of the low Arctic is covered with shrubs that are partially buried by snow in winter and become exposed during melt. This study presents measurements and modeling of shortwave radiation reflection and extinction by a deciduous shrub canopy emerging from a melting snowcover in the mountains of the Yukon Territory, Canada. Shrubs shade most of the snow surface at low solar elevation angles, so only a fraction of the incoming radiation reaches the surface, but there is greater direct shortwave transmission to the surface in gaps between shrubs for higher solar elevations. A simple model is developed to incorporate the changing contributions of sun-lit gaps, shaded gaps, and shrubs to the landscape-averaged (areal) transmission and reflection of shortwave radiation. The areal transmissivity and albedo in this model are lower than in a two-stream approximation that neglects gap shading. A simple shadow parameterization is proposed for calculating shrub tundra snowmelt rates and surface energy balances in hydrological and land-surface models.

DOI: 1657/1523-0430(06-023)[BEWLEY]2.0.CO;2

Introduction

Shrubs coexist with seasonal snowcover over much of the subarctic and form the dominant land cover in northern Alaska, the Canadian low Arctic, and parts of Siberia (DeFries et al., 1998). Tape et al. (2006) presented evidence of increasing shrub abundance in Arctic Alaska by comparing pairs of historical and modern photographs (taken in 1950 and 2000, respectively) of the same areas in Arctic Alaska, finding that detectable shrub increases occurred in 87% of the photographic pairs, and the majority of remaining pairs suggesting no change had occurred. This evidence is further supported throughout the Arctic by a number of satellite remote sensing studies (e.g. Jia et al., 2003). Two of the three fastest warming regions on the planet in the last few decades have been Alaska and Siberia (NERC, 2005), and Epstein et al. (2004) suggested that the shrubs characterizing the transitional area between shrub-tundra and tussock-tundra are sensitive indicators of climate warming and appear to be the most responsive ecosystem to climatic warming over a wide range of tundra and treeline biomes considered. Snow accumulation and melt rates in shrub tundra may be substantially higher than in sparse tundra (Pomeroy et al., 2006; Sturm et al., 2005) and have been shown to control the timing and peak of streamflow in upland tundra headwater basins (McCartney et al., 2006).

Subarctic shrub tundra consists primarily of open to closed birch or willow canopies (Jorgenson and Heiner, 2004); species studied in other shrub-snow field investigations include *Betula nana* and *Salix pulchra* (Sturm et al., 2005), and *Betula glandulosa* (N. Cuthbert, personal communication). Closed shrub canopies are represented in land surface models as a homogeneous vegetation cover, with a set of parameter values specific to shrubs (e.g. Raupach et al., 1997; Essery et al., 2003), and the shortwave radiative transfer algorithms associated with this canopy can be relatively simple. Although dual-source schemes exist to parameterize heterogeneity associated with open shrub canopies (e.g. Blyth et al., 1999), these have been developed for arid or semiarid areas in which the vegetated fraction and density are relatively constant over time. These schemes also commonly employ two-stream approximations when simulating shortwave radiation transfer through canopies, considering only vertical fluxes and neglecting shadows cast across the landscape. Gryning et al. (2001) demonstrated that heat fluxes over a sparse coniferous forest are controlled more by the shading effect of the trees and are not very sensitive to the actual fraction of the surface occupied by forest. Shading of gaps will clearly influence the energy balance of partially vegetated surfaces under direct illumination, with a balance between increasing radiation and decreasing shading with increasing solar elevation.

In contrast with simple models used for continuous canopies, complex physically based models such as GORT (Ni et al. 1997) and TSETSE (Roujean, 1999) have been developed to simulate the processes of shortwave radiation transmission and reflection through open forest canopies (e.g. Woo and Giesbrecht, 2000). These commonly use a combination of geometrical optics and radiative transfer schemes to account for extinction by canopy elements and the influence of canopy gaps on transmittance through the canopy. However, these models require parameters that are not routinely measured as part of forest inventory descriptions (Nijssen and Lettenmaier, 1999), and their application is limited to highly focused research investigations. A similar study of the radiation attenuation within deciduous subarctic shrub canopies, of relatively low foliage density, continuity, and height in comparison to forests, has yet to occur and forms the focus of this study.

It is the purpose of this paper to improve the understanding of solar radiation transfer through a subarctic shrub canopy. Structural and radiative measurements for one such canopy are outlined and then used to run a simple radiative transfer model developed to simulate the areal transmissivity and albedo of an emerging discontinuous deciduous canopy. Comparisons with

1523-0430/07 $7.00

measurements indicate that the model's ability to simulate shaded gap areas gives improved predictions of overall shortwave irradiance at the snow surface, relative to a two-stream approximation in which no gap shading occurs. Finally, a simple parameterization of the fraction of shading that may be applied in shrub snowmelt models, requiring only simple canopy statistics, is developed.

Field Site and Measurements

Field measurements were conducted in the 195 km^2 Wolf Creek Research Basin (60°35′N, 135°11′W; Fig. 1), which lies in the mountainous southern headwaters of the Yukon River in northwestern Canada. The subarctic continental climate is characterized by a large seasonal variation in temperature, low relative humidity and relatively low precipitation. Mean annual temperature is −3°C, and annual precipitation is 300–400 mm, with approximately 40% falling as snow. Wolf Creek is situated within the Boreal Cordillera ecozone (Environment Canada, 1995) and consists of three principle ecosystems: boreal forest (800–1500 m a.s.l.), shrub-tundra (1500–1800 m a.s.l.), and alpine tundra (1800–2400 m a.s.l.) covering 22, 58, and 20%, respectively, of the basin area (Fig. 1). The shrub-tundra zone is snow-covered from early October to May, with snowdrifts persisting until June.

The field site was near 1400 m a.s.l. in the 8 km^2 Granger Creek sub-basin. A 30 m × 30 m (900 m^2) valley-bottom area was selected, and intensive field measurements were conducted there during the 2003 and 2004 melt seasons. The alder (*Alnus crispa*) shrubs (Fig. 2) in this area have predominantly vertical branches, retain marcescent leaves in the upper parts of the canopy, and become exposed during the melt season both gradually as snow ablates and rapidly by spring-up of buried branches (Pomeroy et al. 2006). In high snowfall years, many of the shorter shrubs (<1 m) are completely buried prior to melt. At higher elevations, away from the drainage courses in the valley bottom, shrubs are either absent or dominated by *Salix* species of limited height (<0.6 m).

The study grid was subdivided into 5 m × 5 m cells for measurement of canopy structure and snow depth. At the nodes of this grid, snow depth was measured on days 112, 122, 127, and 132 in 2004 (21 April and 1, 6, and 11 May, respectively), and upward-looking hemispherical photographs were taken on days 112, 122, and 129. Plant area index PAI (the ratio between the total plant surface area and the surface area of ground that is covered by plants; Table 1) and sky-view factor v_f (the fraction of the sky hemisphere not blocked by shrubs) were calculated from the hemispherical photographs using the Gap Light Analyzer (GLA; Frazer et al., 1999). When the shrubs were fully exposed after the main melt period, four shrubs were selected at random in each cell and measured for maximum height and width. Additionally, a high-resolution digital aerial photograph was taken from a remote-controlled helicopter directly above the study grid on day 129 after a light snowfall (see inset, Fig. 1). This aerial photograph is particularly useful because all the shrubs were exposed by this date, and the snowcover in the gaps contrasts strongly with the shrubs.

Shortwave radiation was measured in 2003 by 10 Matrix pyranometers, one above the canopy and the others on the snow

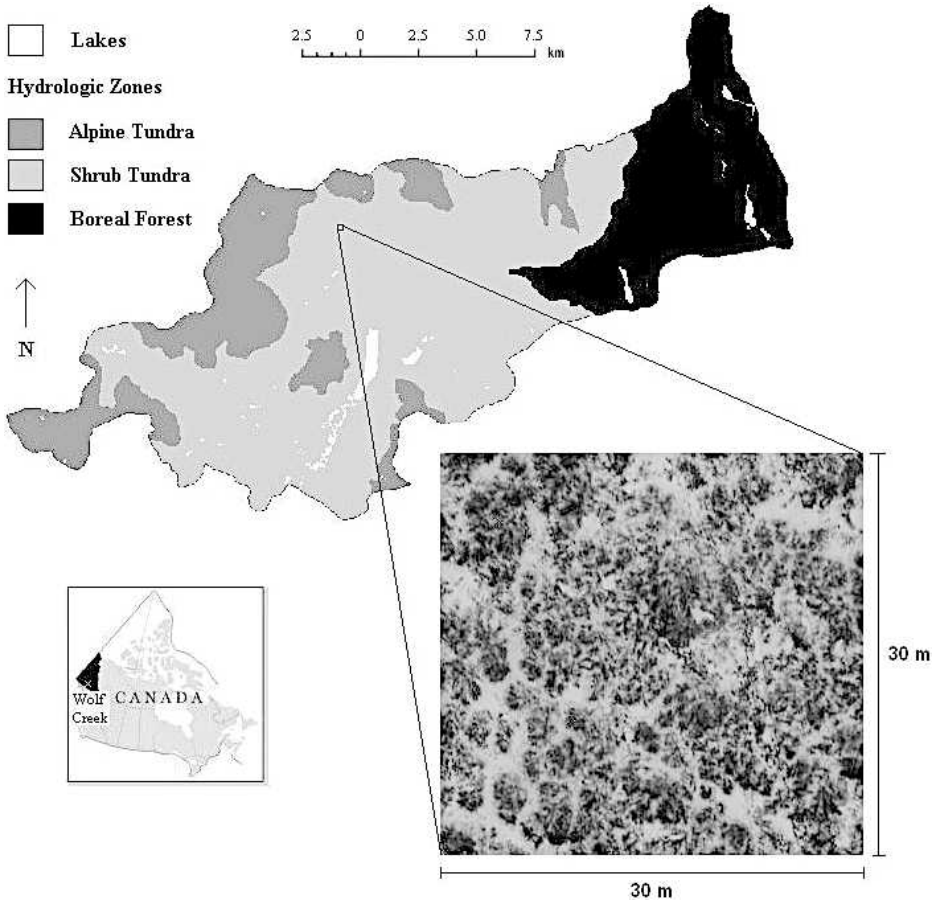

FIGURE 1. Location and ecosystem zones of the Wolf Creek Research Basin, and (inset) an aerial photograph of the study grid showing exposed shrubs and ground snowcover on 8 May 2004.

FIGURE 2. Alder shrubs exposed above the snowpack (background) and individual branches just prior to spring-up (foreground). South is to the left of the picture.

surface beneath shrubs of varying heights (1.0–2.3 m) and densities (PAI 0.5–1.1), allowing calculation of transmission through the shrubs. Reflected radiation was measured with upwards- and downwards-looking pyranometers over a large snow patch with no exposed vegetation or nearby shrubs and above a large mass of cut shrub branches completely covering the ground. Albedos of pure snow and pure shrubs were calculated from these observations. The measured albedo of the sun-lit snow surface was found to be 0.85 when averaged over the daytime period of data collection (range 0.81–0.90, standard deviation 0.04), with lower values measured at higher solar elevations. Similarly, the measured diurnal mean shrub albedo was 0.11 (range 0.10–0.17, standard deviation 0.02), although directly comparable values of snow and shrub albedos in overcast conditions could not be obtained.

Field Results

STRUCTURAL MEASUREMENTS

The pattern and fraction of shrub cover on day 129 were calculated from the aerial photograph. Shrubs were differentiated from snow by applying an intensity threshold to the image to produce a binary mask (see Fig. 6) and adjusting the threshold subjectively to match the pattern of exposed shrubs. The chosen digital number (DN) threshold of 103 gives a shrub fraction F_v of 71.4% and a gap fraction F_o of 28.6%; decreasing or increasing the threshold by an arbitrary figure of 10 changes F_v to 80.1% or 64.2%, respectively.

Aerial photographs are not available for earlier dates during melt, but F_v can also be estimated from hemispherical photographs. Each fisheye photograph taken on day 129 was divided into nine 10° zenith rings, and the gap fraction was calculated for each ring. Classifying photographs as representative of shrub-covered points if branches were apparent in rings at elevation angles of 50° or greater and dividing the number of such photographs by the total number of photographs in the grid (49) was found to match the value of F_v estimated from the aerial photograph. Applying the same criterion to grids of hemispherical photographs taken on days 112 and 122 gives F_v values of 20.4% and 30.6%, respectively (Table 2).

PAI values were calculated using GLA for each shrub-covered image and averaged for each observation date to assess how the mean PAI for the shrub fraction changed with increased shrub exposure as the snow melted. The remaining photographs, considered to be representative of canopy gaps, were analyzed to obtain an average sky-view factor for the gaps. Resulting values of PAI and v_f are given in Table 3.

RADIATIVE MEASUREMENTS

Figure 3 shows the measured global shortwave irradiance ($S_{\downarrow 0}$) for days 121 (clear) and 122 (overcast). A limited number (222) of diffuse radiation measurements made using a shadow ring at a nearby site were used to calibrate the model of Pohl et al.

TABLE 1

List of symbols.

Symbol	Explanation
F_l	Lit fraction of canopy gaps
F_o	Open (gap) fraction of the landscape
F_s	Shaded fraction of canopy gaps
F_v	Vegetated (exposed shrub) fraction of landscape
H	Exposed shrub height
K	Extinction coefficient
l_p	Canopy path length
l	Shadow length
L	Gap length
PAI	Plant area index
$S_{\downarrow 0}$	Downwards shortwave radiation above the canopy
$S_{\downarrow \mathrm{B}}$	Direct-beam downwards shortwave radiation
$S_{\downarrow \mathrm{D}}$	Diffuse downwards shortwave radiation
$S_{\downarrow l}$	Downwards shortwave radiation in lit canopy gaps
$S_{\uparrow l}$	Upwards shortwave radiation above lit canopy gaps
$S_{\downarrow s}$	Downwards shortwave radiation in shaded canopy gaps
$S_{\uparrow s}$	Upwards shortwave radiation above shaded canopy gaps
$S_{\downarrow v}$	Downwards shortwave radiation beneath vegetation
$S_{\uparrow v}$	Upwards shortwave radiation above vegetation
$S_{\downarrow AREAL}$	Spatial-average downwards shortwave radiation at the surface
v_f	Sky-view factor
W	Shrub width
α_s	Snow albedo
α_v	Vegetation albedo
α_{AREAL}	Effective areal albedo
θ	Solar elevation angle
σ_H	Standard deviation of shrub height
σ_L	Standard deviation of gap length
τ	Shortwave transmissivity
τ_{AREAL}	Effective areal transmissivity

TABLE 2

Image thresholds and vegetation fractions estimated from the aerial photograph (day 129) and hemispherical photographs (days 112 and 122).

Day	DN threshold	F_v
112	50	0.204
122	61	0.306
129	103	0.714

TABLE 3

Bulk values of PAI (area F_v), v_f (F_o), and τ (F_v) calculated for days 112, 122, and 129 of 2004. Standard deviations and numbers of images classified as shrub-covered or gaps are also given for PAI and v_f.

Day:		112	122	129
PAIz	Mean	0.41	0.49	0.60
	σ	0.01	0.07	0.13
	N_{shrub}	12	16	37
v_f	Mean	0.77	0.70	0.59
	σ	0.05	0.05	0.05
	N_{gap}	37	33	12
τ		0.69	0.64	0.57

(2006), which estimates direct-beam irradiance ($S_{\downarrow B}$) and diffuse irradiance ($S_{\downarrow D} = S_{\downarrow 0} - S_{\downarrow B}$) from solar elevation angle θ and the ratio of $S_{\downarrow 0}$ to the extra-terrestrial irradiance; $S_{\downarrow B}$ and $S_{\downarrow D}$ estimates are also shown in Figure 3.

A shortwave transmissivity τ can be defined for each sub-canopy radiometer as the fraction of the incident radiation penetrating the canopy. Averages of transmissivities for four radiometers placed at the base of shrubs are shown in Figure 4 as functions of solar elevation for two cases: clear sky day 129 (2003) when direct-beam radiation dominated ($\bar{\tau} = 0.44$), and overcast day 133 with only diffuse light ($\bar{\tau} = 0.45$). Little relationship is observed between τ and θ for either day ($r^2 = 0.09$ and 0.49, respectively), as predicted for horizontally orientated shrub branches (Ross, 1975). The variability in τ was greater under clear skies, as changes in solar position cause rapid movement of shadows across the radiometers. Some hysteresis is apparent in Figure 4 because the sampled transmissivity has a slight

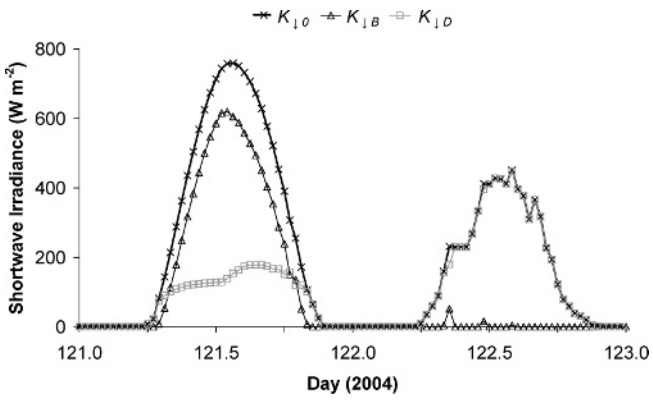

FIGURE 3. Measured global shortwave radiation ($S_{\downarrow 0}$) and estimated direct-beam ($S_{\downarrow B}$) and diffuse ($S_{\downarrow D}$) components on clear and overcast days.

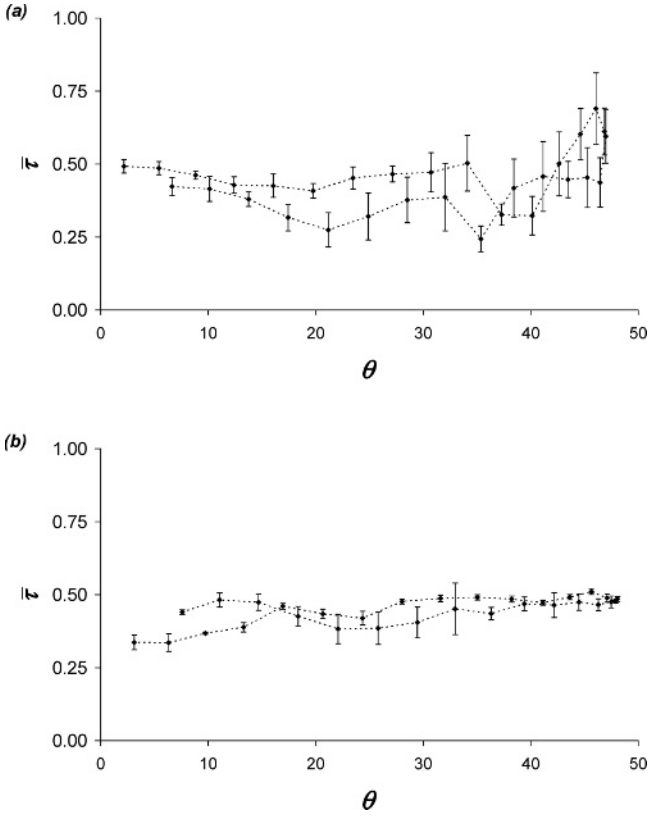

FIGURE 4. Observed mean transmissivity ($\bar{\tau}$) and solar elevation (θ) for (a) clear-sky day 129 and (b) overcast day 133 in 2003. Vertical bars extend to ± one standard deviation.

dependence on solar azimuth and the irradiance was slightly higher in the afternoons than the mornings for the same solar elevations.

Model Descriptions

TWO-STREAM MODEL

Radiation schemes in atmospheric models and canopy schemes in land-surface models typically use two-stream approximations representing vertical downwards and upwards fluxes of radiation (e.g. Blyth et al., 1999). Horizontal influences of shadows cast by vegetation canopies onto canopy gaps are not represented in the strictly vertical two-stream framework.

The two-stream model used here is taken from the dual-source model of Blyth et al. (1999) for sparse vegetation. The open fraction of the surface receives the full incident shortwave irradiance without obstruction by vegetation. The shortwave irradiance at the surface under the canopy $S_{\downarrow v}$ comprises radiation transmitted through the canopy and multiple reflections between the snow and the overlying canopy, giving

$$S_{\downarrow v} = \frac{\tau(1 - \alpha_v)}{1 - \alpha_v \alpha_s} S_{\downarrow 0} \quad (1)$$

where α_v is the vegetation albedo and α_s is the snow albedo. The areal average shortwave radiation at the surface for a landscape with shrub fraction F_v and open fraction $F_o = 1 - F_v$ is then

$$S_{\downarrow AREAL} = F_o S_{\downarrow 0} + F_v S_{\downarrow v} \quad (2)$$

and the areal transmissivity is

$$\tau_{AREAL} = \frac{S_{\downarrow AREAL}}{S_{\downarrow 0}} \tag{3}$$

The outgoing flux of radiation above the canopy is

$$S_{\uparrow v} = \left[\alpha_v + \frac{\tau^2(1-\alpha_v)^2\alpha_s}{1-\alpha_v\alpha_s}\right] S_{\downarrow 0} \tag{4}$$

which includes radiation reflected directly from the canopy and radiation transmitted upwards through the canopy after multiple reflections from the surface.

SHADING MODEL

The radiative transfer model developed here is intended to simulate the transmission of shortwave radiation to a snowpack masked by a discontinuous shrub canopy more faithfully by including the influences of shrub shadows cast onto gaps between shrubs and multiple reflections between snow in the gaps and the canopy. Three landscape fractions are represented in the model, as illustrated in Figure 5, and a separate description of shortwave transmission and reflectance is used for each. Shrubs cover fraction F_v of the surface and are semi-transparent, allowing some light to penetrate to the surface. Shadows cast by shrubs on adjacent gaps cover fraction F_s, and the remaining sun-lit portions of the canopy gaps cover fraction $F_l = 1 - F_s - F_v$. The transfer schemes applied to each are described below.

Fraction F_l initially receives the full direct component and diffuse radiation from the visible part of the sky, giving

$$S_{\downarrow l} = S_{\downarrow B} + v_f S_{\downarrow D} \tag{5}$$

which after single reflections from the snow and the surrounding shrubs becomes

$$S_{\downarrow l} = (1 - v_f)\alpha_v\alpha_s(S_{\downarrow B} + v_f S_{\downarrow D}) \tag{6}$$

and after an infinite series of reflections sums to

$$S_{\downarrow l} = \frac{1}{1-(1-v_f)\alpha_v\alpha_s}(S_{\downarrow B} + v_f S_{\downarrow D}) \tag{7}$$

In the shaded fraction, the snow is only illuminated by diffuse radiation from the sky and radiation transmitted through or reflected from the vegetation, giving

$$S_{\downarrow s} = \frac{1}{1-(1-v_f)\alpha_v\alpha_s}(\tau S_{\downarrow B} + v_f S_{\downarrow D}) \tag{8}$$

Shortwave radiation to the snow surface beneath shrubs is given by the same expression as in the two-stream model, assuming equal transmissivities for $S_{\downarrow B}$ and $S_{\downarrow D}$ so that

$$S_{\downarrow v} = \frac{\tau(1-\alpha_v)}{1-\alpha_v\alpha_s}(S_{\downarrow B} + S_{\downarrow D}) \tag{9}$$

Weighting by the fractional areas covered by each surface type, the average irradiance at the snow surface is

$$S_{\downarrow AREAL} = F_l S_{\downarrow l} + F_s S_{\downarrow s} + F_v S_{\downarrow v} \tag{10}$$

and the areal transmissivity is

$$\tau_{AREAL} = \frac{S_{\downarrow AREAL}}{S_{\downarrow B} + S_{\downarrow D}} \tag{11}$$

The shortwave radiation reflected from the vegetated fraction is given by Equation (4), and the reflected radiation from the sun-lit and shaded gap fractions are simply

$$S_{\uparrow l} = \alpha_s S_{\downarrow l} \tag{12}$$

and

$$S_{\uparrow s} = \alpha_s S_{\downarrow s} \tag{13}$$

The effective areal albedo is then

$$\alpha_{AREAL} = \frac{F_l S_{\uparrow l} + F_s S_{\uparrow s} + F_v S_{\uparrow v}}{S_{\downarrow B} + S_{\downarrow D}} \tag{14}$$

Shaded areas are calculated using a method similar to that suggested by Granberg (1988) for forests. The shrub mask obtained from the aerial photograph is divided into horizontal slices that are then projected along the direction of the solar beam until they intersect the surface; shadows are thus defined by the projections of the shrubs onto the surface. Shaded snow adjacent to and under the exposed shrubs is given an effective albedo of 0.75, lower than was measured in the field under sun-lit conditions. This follows from the work of Melloh et al. (2002), who noted a small reduction in snow albedo under a forest due to preferential absorption of visible radiation (more strongly reflected from snow) by the canopy, and from Hardy et al. (1998), who observed a further reduction due to leaf litter in the snow. Buried shrub branches can also absorb radiation penetrating the snow.

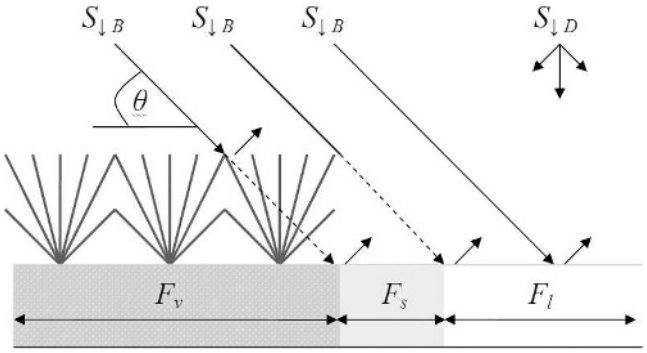

FIGURE 5. Landscape fractions and illumination in the shading model.

PARAMETERIZATION OF TRANSMISSIVITY

Models differ in how they parameterize transmissivity (e.g. Yamazaki et al., 1992; Pomeroy and Dion, 1996), but generally assume that it is an exponential function of PAI, giving

$$\tau = e^{-K\,PAI}, \tag{15}$$

where the extinction coefficient K depends on θ, path length through the canopy and canopy structure. For a continuous canopy of height H, as considered in most models, the path length is

$$l_p = \frac{H}{\sin\theta}, \tag{16}$$

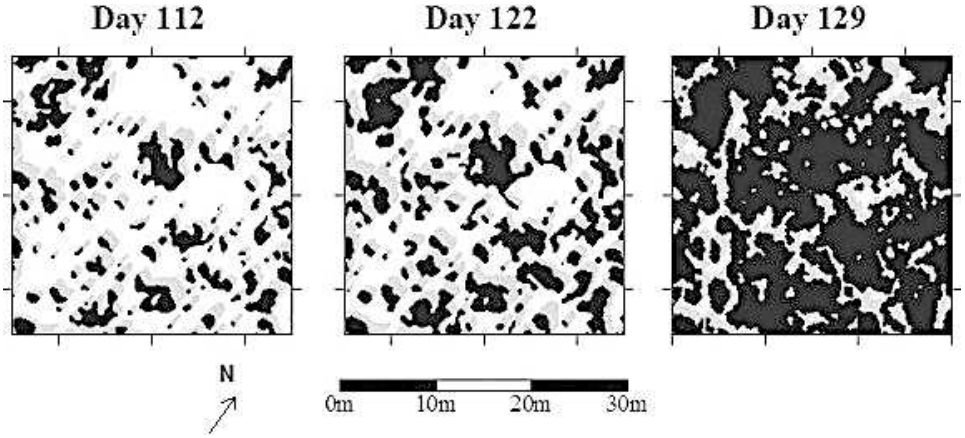

FIGURE 6. Simulated areas of sunlit snow (white), shaded snow (gray), and exposed shrubs (black) at 13:00 (local solar noon) for days 112, 122, and 129 under clear-sky conditions.

but this is not the case for discontinuous canopies. Instead, we derive an effective K from averages of τ and PAI measured at shrub bases as

$$K = -\frac{\ln\bar{\tau}}{\mathrm{PAI}} \tag{17}$$

It was found above that measured transmissivities for direct and diffuse radiation are approximately equal and have little dependence on θ. The average value of K is therefore used in both the two-stream and shading models, giving

$$\bar{\tau} = e^{-0.92\,\overline{\mathrm{PAI}}} \tag{18}$$

There may be site specific variations in the effective K, and further work is necessary to evaluate extinction as a function of shrub geometry, length scale, stem angle, and solar angle in sparse canopies.

Model Results

SHADED AREAS

Simulations were performed using parameter values, given in Table 3, derived from observations for days 112, 122, and 129 in 2004. Shaded areas were simulated on a grid with the same 3.5 cm pixel size as the aerial photograph. Since an aerial photograph was only available for day 129 and heights were only measured for a sample of 144 shrubs, grids of vegetation cover and height had to be constructed for each date. Measured shrub heights were interpolated by kriging (using a linear model and a nugget fitted to the experimental variogram) to generate a shrub height field, which was then reduced by the area-average snow depth measured on each date to simulate exposed shrub heights; this may underestimate the height for shrubs bent over by snow, but insufficient information is available on the spring-up mechanism as yet. Shrub masks were manufactured for days 112 and 122 from the day 129 aerial photograph by applying lower threshold values, given in Table 2, adjusted to fit F_v values calculated from the hemispherical photographs. This relies on the observation that taller and denser parts of the shrub clumps, which will emerge first from the melting snow, appear darker in the photograph.

Shadows were simulated with appropriate solar elevations and azimuths at half-hourly intervals. Figure 6 shows exposed shrubs and simulated shadows at 1300 h (local solar noon) when the shaded fraction is minimized. The landscape progresses from a gap-dominated environment before melt commences to a shrub-dominated environment as the shrubs are progressively exposed by the receding snowpack. This transition occurred at some point between days 122 and 129 in 2004.

Figure 7 shows calculated gap-shaded fraction F_s and sun-lit fraction F_l as functions of solar elevation for days 112 and 129. F_l approaches zero when the shrubs cast long shadows at low θ. On day 112, when the shrubs still have small exposed areas and heights above the snowpack, F_l rises rapidly after the sun rises above the horizon, and sun-lit snow patches dominate the landscape for $\theta \geq 22^\circ$. A maximum of $F_l = 0.60$ is obtained at solar noon, at which time $F_s = 0.20$. Spatial variations in shrub density lead to slightly lower amounts of shadow being cast across the area in the morning than for the same solar elevations but different azimuths in the evening. On later dates, as the exposed shrubs increase in abundance and height, the decreasing canopy gap area decreases both F_l and F_s, and F_l has become an insignificant fraction of the landscape by day 129 ($F_l = 0.07$ at solar noon); canopy gaps remaining during the latter stages of melt are increasingly shaded by the shrubs.

AREAL TRANSMISSIVITY

The two-stream model requires global shortwave irradiance data, which was measured, but the shading model requires separate diffuse and direct shortwave irradiance; these are estimated using the model of Pohl et al. (2006), as described above.

Figure 8 shows τ_{AREAL} simulated by the shading and two-stream models on days 112 and 129, assuming clear skies. On day 112, the two-stream model simulates a high τ_{AREAL} (0.93), since 79.6% of the landscape consisted of canopy gaps (where $\tau = 1$) and the remaining exposed shrub fraction had a high transmissivity (0.67) due to the low pre-melt PAI. In the shading model, a minimum in $\tau_{AREAL} = 0.75$ is simulated at low θ when the

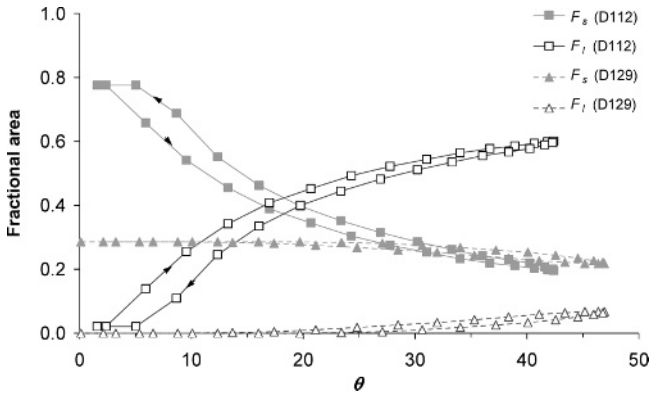

FIGURE 7. Fractional areas of shaded and sunlit snow as functions of solar elevation on days 112 and 129.

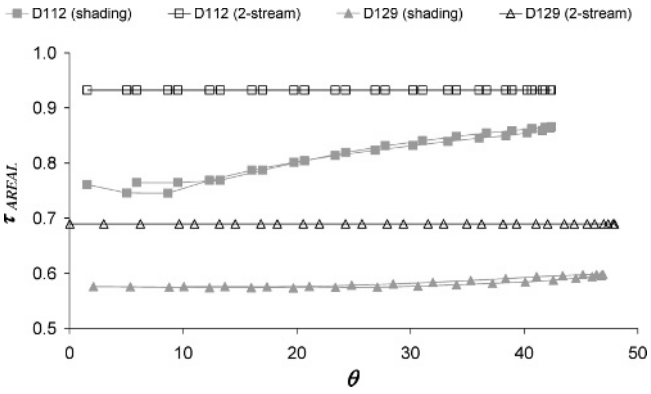

FIGURE 8. Dependence of τ_{AREAL} on θ in the shading and two-stream models for days 112 and 129 under clear-sky conditions.

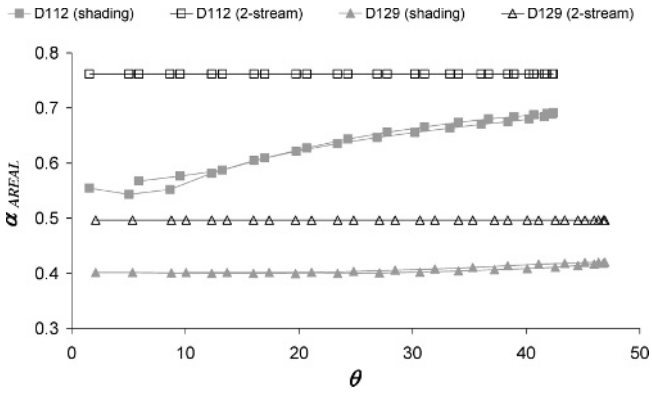

FIGURE 9. As Figure 8, but for α_{AREAL}.

canopy gaps are almost entirely shaded; for shorter shadow lengths at higher θ, τ_{AREAL} increases to a maximum of 0.87 at solar noon ($\theta = 42^{\circ}$). τ_{AREAL} would tend further toward (but not exactly to) the two-stream result if θ were higher. The slight hysteresis, with τ_{AREAL} higher for a given θ in the afternoon than in the morning, is due to the increased diffuse component during the afternoon being more efficiently transmitted to the shaded gap fraction than the direct component (since $v_f > \tau$). Of the measured daily total of 23.9 MJ m^{-2} incoming solar radiation, 22.3 MJ m^{-2} is transmitted to the surface by the two-stream model and 20.0 MJ m^{-2} by the shading model; τ_{AREAL} is therefore 0.09 lower on average (half-hourly values up to 0.18 lower) when simulated using the shading model.

For overcast conditions, irradiance in gaps is not influenced by shadows but is still lower in the shading model than the two-stream model due to restriction of the sky view. The transmissivity to snow beneath shrubs remains unchanged from the clear-sky simulation (0.67), since the models transmit diffuse and direct light identically in this fraction, and τ_{AREAL} remains constant at 0.76 in the shading model. The two-stream model in effect transmits global radiation for all fractions, and the τ_{AREAL} result of 0.93 is therefore unchanged from the clear-sky simulation. Shortwave radiation (12.6 MJ m^{-2}) was measured above the canopy, 9.6 MJ m^{-2} is transmitted to the snow surface by the shading model, and 11.6 MJ m^{-2} by the two-stream model.

By day 129, τ_{AREAL} simulated by both models in clear-sky conditions is reduced by the extensive F_v fraction (71.4%) of higher PAI and the resulting reduction of canopy gaps with variable shaded and sun-lit fractions. τ_{AREAL} from the shading model rises from 0.57 at low θ to 0.60 at solar noon (average 0.59), and 14.0 MJ m^{-2} of shortwave radiation is transmitted to the snow surface (72% of the amount on day 112). The two-stream model simulates a constant τ_{AREAL} of 0.67, and 16.1 MJ m^{-2} is transmitted (70% of the day 112 value). For overcast simulations, 7.2 MJ m^{-2} ($\tau_{AREAL} = 0.58$) and 8.7 MJ m^{-2} ($\tau_{AREAL} = 0.69$) is transmitted by the shading and two-stream models, respectively.

AREAL ALBEDO

Figure 9 shows α_{AREAL} on days 112 and 129 for clear skies. For day 112, α_{AREAL} in the shading model rises from 0.54 at low θ to 0.69 at solar noon (average 0.66) due to the decrease of shading in gaps and the increasing availability of direct radiation for reflection. Neglecting shaded gaps, the two-stream model produces a constant $\alpha_{AREAL} = 0.76$, which is only 0.09 less than that for complete snowcover since the exposed shrub fraction remains small and moderately transparent. By day 129, the considerably increased shrub area and density decrease the albedo of the shrub fraction to 0.35, and the diurnal range of the areal albedo in the shading model is limited (0.40–0.42). The average value of 0.41 is approximately the same as in overcast conditions (0.40), and the two-stream result of $\alpha_{AREAL} = 0.50$ holds for either clear or overcast conditions.

COMPARISON WITH OBSERVATIONS

Too few radiometers were available in 2004 to evaluate simulated areal transmissivities and albedos directly. Although aerial photography was not available to generate shrub grids for 2003, however, there were sufficient subcanopy radiometers to estimate an observed τ_{AREAL}. An average irradiance under the canopy was calculated for clear-sky day 129 in 2003 from four radiometers placed centrally at the base of shrubs and a further five deployed to the side of shrubs and in canopy gaps. Figure 10 shows a comparison of the calculated τ_{AREAL} against simulations using parameter values for day 129 in 2004 (Table 3). The shading model (rms error 0.07, average error 0.01) gives better results than the two-stream model (rms error 0.14, average error 0.08). However, the shading model overestimates τ_{AREAL} at lower solar angles and underestimates the diurnal range. The simulated range of τ_{AREAL} is larger for earlier stages in melt (Fig. 8), indicating a potentially incorrect specification of the exposed shrub fraction and structure by assuming that values for day 129 in 2003 were the same as those measured in the field one year later. Despite this, these results indicate that the shading-model can simulate

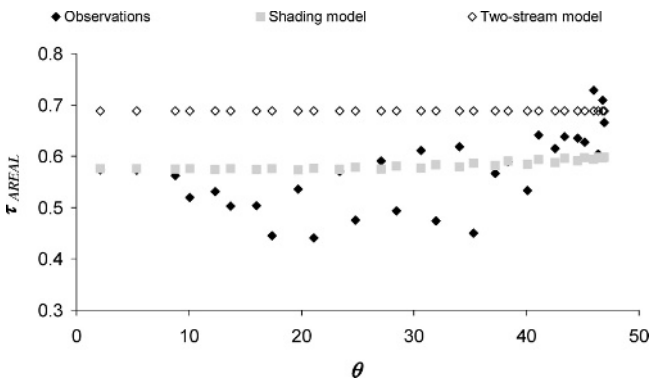

FIGURE 10. Simulated and observed τ_{AREAL} for day 129 in 2003.

shortwave transmission (and potentially reflection) from a discontinuous shrub canopy better than a two-stream approximation.

Parameterization of Shadow Fractions

The shading model predicts patterns of shadow over a landscape with discontinuous shrub cover, but it is computationally expensive and requires a detailed map of shrub heights. For practical applications, a parameterization giving a rapid calculation of the shaded fraction of the landscape from a small number of parameters is required.

Consider a shrub of height H and width W. The length of the shadow cast by this shrub when the sun is at elevation θ is $l = H/\tan\theta$. If l exceeds the gap distance L to the next shrub in the shaded direction, the shrub shadows overlap. The fraction of the landscape covered by shadows in gaps is

$$F_S = \frac{\bar{l}}{\bar{W} + \bar{L}} \tag{19}$$

where $\bar{l}$, $\bar{W}$, and $\bar{L}$ are the averages of l, W, and L over the landscape (measured values of $\bar{W}$ and $\bar{L}$ are presented in Table 4). Allowing for overlap of shadows, the average shadow length is given by

$$\bar{l} = \int\int dH\, dL\, p(H, L)\min\left(\frac{H}{\tan\theta}, L\right) \tag{20}$$

where $p(H,L)$ is the joint probability distribution of H and L. From the surveyed shrub heights and gap lengths measured from the aerial photograph, it was found that H and L are uncorrelated, so the joint distribution can be replaced by the product of their individual distributions. Moreover, it was found that the distributions can be approximated by a normal distribution

$$p_H(H) = \frac{1}{\sqrt{2\pi}\sigma_H}\exp\left[-\frac{(H - \bar{H})^2}{2\sigma_H^2}\right] \tag{21}$$

for H and a lognormal distribution

$$p_L(L) = \frac{1}{\sqrt{2\pi}L\sigma_y}\exp\left[-\frac{(\ln L - \bar{y})^2}{2\sigma_y^2}\right] \tag{22}$$

for L, where

$$\sigma_y^2 = \ln\left[1 + \left(\frac{\sigma_L}{\bar{L}}\right)^2\right] \tag{23}$$

and

$$\bar{y} = ln\bar{L} - \frac{\sigma_y^2}{2} \tag{24}$$

σ_H and σ_L are the measured standard deviations of H and L (Table 4). Numerical integration of Equation (20) and substitution in Equation (19) then gives an efficient prediction of the shaded fraction. Figure 11 compares this parameterization with results from the shading model for varying solar elevations using the vegetation grids for days 112 and 129. The r^2 and rms errors

TABLE 4

Input variables for the parameterized shading model.

Day	$\bar{W}$	$\bar{H}$	σ_H	$\bar{L}$	σ_L
112	1.024	0.93	0.286	3.725	3.595
122	1.295	1.196	0.286	2.810	2.467
129	2.742	1.546	0.286	1.172	1.103

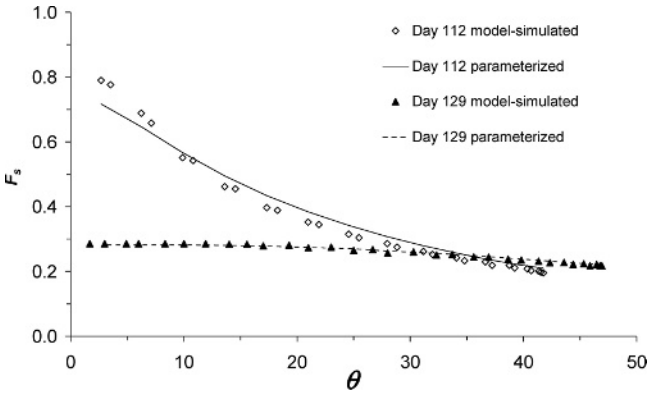

FIGURE 11. Simulated and parameterized shaded gap fractions for days 112 and 129.

are 0.995 and 0.016 (day 112), and 0.996 and 0.008 (day 129), respectively.

The parameterized version of the shading model can be run for discontinuous shrub canopies with only basic information about canopy characteristics. An aerial photograph of the study area, of sufficiently high resolution to delineate individual shrub patches and canopy gaps, provides the most rapid method for obtaining this information. Image-analysis software (e.g. Sigmascan, Systat Inc.) can readily compute the required statistics and distributions of shrub width and gap length, and shadow lengths in the image during clear-sky conditions can be inverted trigonometrically to derive the heights. Height distributions might also be obtained from airborne LIDAR data, although height data will be uncertain if returns are not obtained from the highest points of shrubs. The default distributions of shrub heights and gap lengths can easily be replaced by alternative distributions found to be more appropriate for other areas. An important consideration is the landscape area over which the shading model is to be run and environmental controls on shrub cover in this area (e.g. topography and drainage).

The shading model may also be used with hypothetical parameters in sensitivity studies to investigate the influence of shrubs or changes in shrub distribution on the surface energy balance. As an example, Figure 12 shows differences in $S_{\downarrow AREAL}$ simulated by the two-stream and shading models for noon on day 112. In Figure 12a, the shrub geometry is kept fixed but the latitude is varied; the difference between the models is a minimum at the latitude in the tropics where the sun is directly overhead (12°N on day 112), rising to a maximum at more northerly latitudes as the shadows lengthen, then decreasing at high latitudes as the incoming radiation decreases. The maximum difference between the models occurs at 66°N for this scenario, so it is not surprising that shading by shrubs is of more concern for this study at 60°35′N than it was for Blyth et al. (1999) at 13°15′N. Figure 12b shows the difference between the models for varying gap fractions; clearly, the difference will disappear for the homogeneous cases of zero or complete shrub cover and peak at some intermediate fraction. Because the maximum solar elevation is 45° and $\bar{W} \approx \bar{H}$ on day 112, the peak occurs at approximately 50% shrub cover in this case.

Conclusions

The transmission of shortwave radiation through discontinuous shrub canopies to an underlying snowcover is a complex but

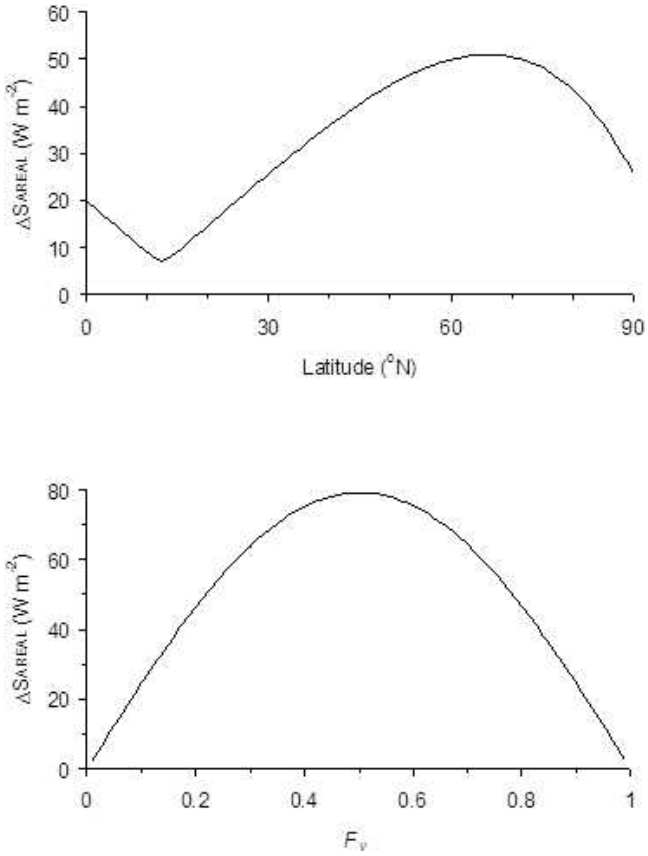

FIGURE 12. Differences in average surface irradiance between the two-stream and shading models for (a) varying latitude and (b) varying shrub fraction at noon on day 112.

important process that can considerably affect the rate of snowmelt. Additionally, the proportion of incident shortwave radiation extinguished by the canopy and not reflected is critical to determining fluxes of heat and moisture to the atmosphere from this landscape. The effective shortwave radiation transmissivity and albedo are substantially different from those for continuous shrub canopies or open snowfields, since the apparent canopy coverage varies considerably with solar elevation.

In this paper, a model has been developed to simulate the effective transmission and reflectance of shortwave radiation from a landscape consisting of a discontinuous shrub canopy over a melting snowpack. The model parameterizes the transmission and reflectance of direct and diffuse shortwave radiation from three landscape fractions: a semi-transparent exposed shrub fraction, and sun-lit and shaded canopy gap fractions. The introduction of shaded canopy gaps contrasts with simpler radiative transfer models in which landscapes are represented by static classes, and it is believed that this method improves the diurnal simulation of shortwave transfer.

Early in the melt period, the direct shortwave radiation transmitted to the snow surface and reflected from the landscape increases considerably as the solar elevation increases, reducing the shading of canopy gaps. Areal transmissivity and albedo were reduced relative to those simulated by a two-stream approximation in which no shading was considered. This reduction is minimized when shrubs are fully exposed and the gap area is small.

To calculate areal transmissivity and albedo for shrub tundra, the shaded landscape fraction can be determined using a parameterization of the shading model with averages and standard deviations of shrub height and gap length and average shrub width as inputs. The height and gap length distributions and statistics required for this calculation can be obtained from high resolution remote imagery, field surveys or informed assumptions. The shrub transmission and snow albedo parameterizations used in the radiative transfer component of the model, however, warrant further investigation. For instance, an improved spatially variable snow albedo scheme to estimate the effects of shrub canopy extinction and buried branches on snow albedo is needed. Also, the extinction coefficients should be parameterized differently for discontinuous shrub canopies, to account for such factors as the effect of shrub and gap dimensions on path length through the canopy. More work is required to parameterize the evolution of exposed shrub heights as shrubs are bent over under snow and spring up during melt.

The areal albedo and transmissivities estimated using the shading model, though physically reasonable and consistent with available observations, could not be verified by areal observations in this study because it was not feasible to deploy sufficient radiometers to characterize such marked spatial distributions. Areal albedo simulations could be evaluated with airborne observations or using radiometers mounted on a sufficiently tall mast to have a footprint including canopy and gap areas. The shortwave radiation scheme will be tested as part of a comprehensive energy-balance model for shrub snowmelt, and areal snow mass balances can then be used to evaluate model performance.

Acknowledgments

We thank all those who contributed to the field experiments, especially Newell Hedstrom and Raoul Granger (Environment Canada); Michael Solohub and Steve McCartney (University of Saskatchewan); Tim Link (University of Idaho); Jean-Emmanuel Sicart and Aled Rowlands (University of Wales, Aberystwyth); and Rick Janowicz, Glen Ford, and Glen Carpenter (Yukon Environment). The loan of the Matrix pyranometer array from Danny Marks (U.S. Department of Agriculture) and Tim Link is greatly appreciated. Wolf Creek Research Basin is operated by the Water Resources Branch, Yukon Department of Environment, and the National Water Research Institute, Environment Canada. This work was supported by Natural Environment Research Council (NERC) Standard Grant NER/A/S/2001/01089. Bewley was supported by NERC Student Grant NER/S/A/2002/10426, Essery by NERC Advanced Research Fellowship NER/J/S/2001/00812, and Pomeroy by a Canada Research Chair. We thank the editor and two anonymous reviewers for their comments on this paper.

References Cited

Blyth, E. M., Harding, R. J., and Essery, R., 1999: A coupled dual source GCM SVAT. *Hydrology and Earth System Science*, 3: 71–84.

DeFries, R., Hansen, M., Townshend, J. R. G., and Sholberg, R., 1998: Global land cover classifications at 8 km spatial resolution: the use of training data derived from Landsat imagery in decision tree classifiers. *International Journal of Remote Sensing*, 19: 3141–3168.

Environment Canada, 1995, *Terrestrial Ecozones of Canada*. Ottawa: Ecological Land Classification Series No. 19.

Epstein, H. E., Beringer, J., Gould, W. A., Lloyd, A. H., Thompson, C. D., Chapin, F. S., Michaelson, G. J., Ping, C. L., Rupp, T. S., and Walker, D. A., 2004: The nature of spatial transitions in the Arctic. *Journal of Biogeography*, 31: 1917–1933.

Essery, R. L. H., Best, M. J., Betts, R. A., Cox, P. M., and Taylor, C. M., 2003: Explicit representation of subgrid

heterogeneity in a GCM land-surface scheme. *Journal of Hydrometeorology*, 4: 530–543.
Frazer, G. W., Canham, C. D., and Lertzman, K. P., 1999: Gap Light Analyzer GLA, Version 2.0: Imaging software to extract canopy structure and gap light transmission indices from true-color fisheye photographs, users manual and program documentation. Burnaby, British Columbia: Simon Fraser University: and Millbrook, NY: Institute of Ecosystem Studies, 40 pp.
Granberg , H. B., 1988: A forest shading model using bit-mapped graphics. *Agricultural and Forest Meteorology*, 43: 225–234.
Gryning, S. E., Batchvarova, E., and de Bruin, H. A. R., 2001: Energy balance of a sparse coniferous high-latitude forest under winter conditions. *Boundary-Layer Meteorology*, 99: 465–488.
Hardy, J. P., Davis, R. E., Jordan, R., Ni, W., and Woodcock, C. E., 1998: Snow ablation modeling in a mature aspen stand of the boreal forest. *Hydrological Processes*, 12: 1763–1778.
Jia, G. J., Epstein, H. E., and Walker, D. A., 2003: Greening of arctic Alaskan, 1981–2001. *Geophysical Research Letters*, 30: 2067.
Jorgenson, T., and Heiner, M., 2004: Ecosystems of northern Alaska. Unpublished Report by ABR, Inc., Fairbanks, AK.
McCartney, S. E., Carey, S. K., and Pomeroy, J. W., 2006: Intra-basin variability of snowmelt water balance calculations in a subarctic catchment. *Hydrological Processes*, 20: 1001–1016.
Melloh, R. A., Hardy, J. P., Bailey, R. N., and Hall, T. J., 2002: An efficient snow albedo model for the open and sub-canopy. *Hydrological Processes*, 16: 3571–3584.
NERC (Natural Environmental Research Council), 2005, *Climate change—Scientific certainties and uncertainties*. Swindon, U.K.: NERC Press.
Ni, W., Li, X., Woodcock, C., Roujean, J. L., and Davis, R. E., 1997: Transmission of solar radiation in boreal conifer forests: measurements and models. *Journal of Geophysical Research*, 102(N24): 29555–29566.
Nijssen, B., and Lettenmaier, D. P., 1999: A simplified approach for predicting shortwave radiation transfer through boreal forest canopies. *Journal of Geophysical Research*, 104: 27859–27868.
Pohl, S., Marsh, P., and Pietroniro, A., 2006: Spatial-temporal variability in solar radiation during spring snowmelt. *Nordic Hydrology*, 37: 1–19.
Pomeroy, J. W., and Dion, K., 1996: Winter radiation extinction and reflection in a boreal pine canopy: measurements and modelling. *Hydrological Processes*, 10: 1591–1608.
Pomeroy, J. W., Bewley, D. M., Essery, R. L. H., Hedstrom, N., Granger, R. J., Sicart, R. E., and Janowicz, R., 2006: Shrub tundra snowmelt. *Hydrological Processes*, 20: 923–941.
Raupach, M. R., Finkele, K., and Zhang, L., 1997: SCAM Soil-Canopy-Atmosphere Model: description and comparisons with field data. Aspendale, Australia: CSIRO CEM Technical Report No. 132, 81 pp.
Ross, J., 1975: Radiative transfer in plant communities. *In* Monteith, J. L. (ed.), *Vegetation and the atmosphere*. London: Academic Press, 13–55.
Roujean, J. L., 1999: Two-story equations of transmission of solar energy TSETSE in open boreal conifer tree stands. *Journal of Geophysical Research*, 104(D22): 27869–27879.
Sturm, M., Schimel, J., Michaelson, G., Welker, J. M., Oberbauer, S. F., Liston, G. E., Fahnestock, J., and Romanovsky, V. E., 2005: Winter biological processes could help convert arctic tundra to shrubland. *BioScience*, 55: 17–26.
Tape, K., Sturm, M., and Racine, C., 2006: The evidence for shrub expansion in northern Alaska and the Pan-Arctic. *Global Change Biology*, 12: 686–702.
Woo, M. K., and Giesbrecht, M., 2000: Simulation of snowmelt in a subarctic spruce woodland: 1. Tree model. *Water Resources Research*, 36: 2275–2285.
Yamazaki, T., Kondo, J., and Watanabe, T., 1992: A heat-balance model with a canopy of one or two layers and its application to field experiments. *Journal of Applied Meteorology*, 31: 86–103.

Ms accepted October 2006